SILICON HALIDE PEROVSKITE FOR EFFICIENT SUNLIGHT HARVESTING IN SOLAR CELLS: INSIGHTS FROM FIRST-PRINCIPLES

MKPENIE, V. AND ABAKEDI, O.
Department of Chemistry, University of Uyo, Uyo, Nigeria.
vicmkpenie1@gmail.com

ISSN: 2141 – 3290
www.wojast.com

ABSTRACT

A silicon-based perovskite was investigated within the framework of density functional theory (DFT) for application in solar energy harvesting technology. The DFT calculations were carried out at GGA-PBEsol and GGA-HTCH/407 level of theory to explore the structural, electronic, and optical properties of the silicon hybrid organic-inorganic perovskite, $CH_3NH_3SiI_3$ ($MASiI_3$) and the results were compared with the popular Pb-containing perovskite, $CH_3NH_3PbI_3$ ($MAPbI_3$). The structure of $MASiI_3$ is indicated as cubic based on the Goldschmidt tolerance factor of 0.93 which is within the range for formation of stable cubic perovskites. It is found that $MASiI_3$ is a direct band gap semiconductor exhibiting *n*–type extrinsic behavior. The optical activities indicate intense absorptions within ultraviolet and visible regions needed for high photovoltaic activity. The high absorption coefficient of $MASiI_3$ within 10^5 is comparable to that of $MAPbI_3$ indicating that the active absorber layer can be structured into a thin film for high power efficiency conversion. The results of this study imply that perovskite absorbers can incorporate silicon (Si) instead of lead (Pb) in an effort to eliminate Pb toxicity that raises environmental concern in hybrid organic-inorganic perovskites (HOIPs).

INTRODUCTION

Perovskite solar cell (PSC) has received increased attention of recent due to its low cost conversion of solar energy into electricity and high power conversion efficiency (PCE). It is a type of solar cell fabricated from a perovskite structured compound having a light-harvesting active layer (Manser *et al*, 2016). Perovskites have been considered as possible inexpensive base materials for high-efficiency commercial photovoltaics and they are inexhaustible since its structure can be easily manipulated to yield various modified versions. A very popular modified version of perovskite is the hybrid organic-inorganic perovskite (HOIP) which has been extensively investigated for commercialization purposes because of an unprecedented increase of the PCE from the initial 3.8% in 2009 (Kojima *et al*, 2009) to the recent certified value of 22.7% (Yang *et al*, 2015). Popular among them is methylammonium (MA) lead trihalide represented as $CH_3NH_3PbX_3$ (or $MAPbX_3$) in which the halide X can be any of I, Br or Cl. It possesses an optical bandgap between 1.5 and 2.3 eV depending on halide content and its effective diffusion lengths are some 100 nm for both electrons and holes (Hodes, 2013).

Although PSCs seem very promising candidates for new-generation photovoltaic absorbers with outstanding intrinsic properties, such as excellent visible-light absorption (Lee et al, 2012), low exciton binding energy (D'Innocenzo *et al*, 2014), high carrier mobility and lifetime (Ponseca *et al*, 2014) and long carrier diffusion length (Stranks *et al*, 2013), they are faced with several critical issues including the presence of toxic lead element in the structure and poor stability upon long-term exposure to moisture and oxygen in the atmosphere. The inclusion of lead as a component of the PSCs expresses an overwhelming concern because of its toxicity at accumulated level in the environment. Effort to move away from lead-based PSCs is ongoing as other metals are being investigated both experimentally and theoretically, including tin (Noel *et al*, 2014), germanium (Krishnamoorthy *et al*, 2015), strontium (Shai *et al*, 2017), cadmium (Navas *et al*, 2015), alkaline-earth metals (Chan *et al*, 2017), and transition metals (Sampson *et al*, 2017). The instability of HOIPs upon exposure to ambient atmosphere is mainly related to environmental influence (moisture and oxygen) (Bryant *et al*, 2016), thermal influence

(intrinsic stability) and heating under applied voltage (Juarez-Perez *et al*, 2016), photo influence (Ultraviolet light) (Yuan *et al*, 2016) and mechanical fragility (Matteocci *et al*, 2016). Several studies about PSCs stability have been performed although there is no standard stability protocol for PSCs (Yuan *et al*, 2016).

Despite the great successes achieved in improved fabrication techniques to produce stable PSCs with high efficiency, understanding their working mechanism remains elusive. This is due to limited experimental tools available for such study. Hence, the use of computational methods have aided our understanding towards the structural and electronic properties of perovskite absorbers (Mosconi *et al*, 2013), and the modeling of photovoltaic properties of perovskites (Arkan and Izadyar, 2018). These theoretical calculations are usually performed with software based on plane-wave basis sets. Although many metals in their +2 oxidation state have been extensively investigated experimentally and theoretically as a replacement for Pb^{2+} ion in the perovskite structure, information on Si^{2+} is clearly lacking despite its favourable ionic radius (analogous to Pb^{2+}). The Goldschmidt tolerance factor for Si^{2+} as B-site atom in halide (iodide) perovskite is well accommodated within the range for the formation of stable perovskite structure.

Herein, we investigate the electronic and optical properties of silicon halide perovskite, $MASiI_3$ using DFT. Si^{2+} may be considered a possible replacement for Pb^{2+} in HOIPs since Pb^{2+} is presumed toxic and environmentally unfavorable. This study is based on first-principles calculation and is intended to reveal interesting properties of $MASiI_3$ as light absorber for use in perovskite solar cell technology.

COMPUTATIONAL METHODS

The crystal structure of cubic $MASiI_3$ was obtained by replacing Pb in cubic $MAPbI_3$ with silicon. The crystal structure of cubic $MAPbI_3$ (c-$MAPbI_3$) was built from experimentally measured lattice parameters (Stoumpos *et al*, 2013): a = 6.313 Å, $\alpha = 90^o$. The cell and atom positions of c-$MAPbI_3$ and c-$MASiI_3$ were fully relaxed using the Dmol^3 (Delley, 2000) module of Materials Studio 2017, implemented within the DFT framework (Kohn and Sham, 1965) with the General Gradient Approximation (GGA) exchange-correlation functional and PBE for solid (PBEsol) (Perdew *et al*, 2008). To optimize the crystal geometry, the convergence tolerance of energy, force and displacement were fixed at $1x10^{-5}$ Ha, $2x10^{-3}$ Ha/Å and $5x10^{-3}$ Å, respectively. Core electrons (electrons in the low lying orbitals) were described in the same manner as valence electrons without any relativistic effect. The double numerical basis set with polarization function (DNP) (Delley, 2006) was utilized with the basis file set to 4.4 to ensure improved accuracy of the calculation. Electronic minimization was facilitated by the use of direct inversion of the iterative subspace (DIIS) (Pulay, 1982). A global cutoff energy was used for the expansion of the plane waves and the k-space integration was done with a 2 × 2 × 2 k-mesh in the Monkhorst−Park scheme (Monkhorst and Pack, 1976). Due to poor band gap obtained from GGA-PBEsol calculation, the band structure was calculated using GGA with non-local functional, HTCH/407 with maximum angular momentum function described by octupole multipolar representation of the charge density (Boese and Handy, 2001). The density of states (DOS) and partial density of states (PDOS) were calculated with denser Monkhorst−Park grid of 4 × 4 × 4 at GGA-HTCH/407. For the calculation of optical properties, the Cambridge Serial Total Energy Package (CASTEP) (Clark *et al*, 2005) module of Materials Studio 2017 was utilized. This was implemented with GGA-PBEsol exchange correlation functional, and OTFG ultrasoft pseudopotentials describing the electrostatic interaction between ionic core and valence electron. A cutoff energy of 517 eV was used for the expansion of the plane waves and the k-space integration was done with a 4 × 4 × 4 k-mesh in the Monkhorst−Park scheme. The optical properties were calculated with 12 bands and 0.38 eV Gaussian smear. The incident radiation for the optical properties was polarized in the (1.0, 0.0, 0.0) direction. This is important for materials that do not display full cubic symmetry.

RESULTS AND DISCUSSION

Structural parameters of $MASiI_3$:

The general cubic structure of HOIPs was adopted for $MASiI_3$. The main crystal framework of $MASiI_3$ is created by placing Si^{2+} and MA^+ at B site and A site, respectively. A single $MASiI_3$ unit cell contains 5 species: 3I, 1C, 1N, 6H, 1Si atoms as shown in Fig. 1a. The Si^{2+} is bonded to three I^- atoms. The calculated lattice parameters using GGA-PBEsol are as follows: a=`5.933 Å, b = 5.777 Å, c = 5.846 Å, α = 88.50º, β = 87.82º, and γ =89.68º and these values deviate from the initial cubic structure (a = 6.313 Å, α = 90º) suggesting some distortion within the crystal structure as Si enters the B site. In order to verify the accuracy of the calculation, the experimental lattice parameters of $MAPbI_3$ were compared with the GGA-PBEsol calculated ones. The GGA-PBEsol calculated lattice parameters for $MAPbI_3$ (a = 6.336 Å, b = 6.332 Å, c = 6.383 Å, α = 89.9º, β = 89.7º and γ = 89.8º) are in agreement with experimental values. Therefore, the lattice parameters of $MASiI_3$ calculated using GGA-PBEsol are reasonably accurate. While the lattice parameters for $MAPbI_3$ are close to cubic, the ones for $MASiI_3$ differ slightly from the cubic, indicating strong anisotropic behaviour. The C-N bond with length 1.630 Å oriented along the X- axis is shortened in the optimized structure to 1.477 Å and the C-N bond axis is rotated about 45º with N atom pointing towards silicon (Fig. 1b). Such reflection is not observed in the optimized geometry of $MAPbI_3$. This may indicate a strong interaction between the cationic organic molecules (MA^+) and the anionic inorganic matrix. With silicon, an interplay between electrostatic and Van der Waals forces may be fundamental to determining the structure and lattice parameters. Although, it is a general believe that there is no bonding interaction between MA and PbI_3 fragments, $MASiI_3$ may present a contrary perspective. The different Si-I bond lengths in the geometry structure is also an indication of anisotropic behavior of $MASiI_3$. The optimized structure showed two short Si-I bonds (3.020 and 2.927 Å) and one long bond (3.175 Å) from the initial Si-I length of 3.156 Å (Fig. 1).

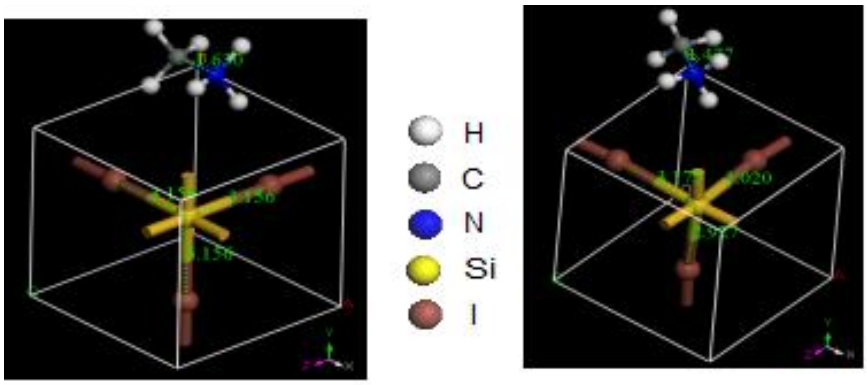

(a) (b)

Figure 1: A unit cell of $MASiI_3$ showing bond length of MA and Si-I (a): Before optimization. (b): After optimization

Stability of $MASiI_3$ structure:

The stability of silicon-based perovskite can be assessed by Goldschmidt tolerance factor according to Eqn (1). The tolerance factor is very useful in describing the ABX_3 structure of perovskites (Liu *et*, 2009) and can indicate stability and distortion.

$$t = r_{MA} + r_I/\sqrt{2}(r_{Si} + r_I) \quad (1)$$

where r_{MA}, r_{Si} and r_X are the ionic radii of MA^+, Si^{2+} and I^-, respectively.

In computing the tolerance factor, the ionic radii of MA^+, I^- and Si^{2+} used were 217 pm (Kieslich *et al,* 2014), 220 pm (Shannon, 1976) and 113 pm (Bhagwan, 2005), respectively. For

values of *t* in the range 0.9-1.0, mostly cubic perovskites are observed. The range 0.8-0.89 shows distorted (Glazer 1972) or orthorhombic perovskites; below 0.8 leads to different structure such as trigonal whereas above 1.0 indicates tetragonal or hexagonal perovskites. The tolerance factor of 0.93 for $MASiI_3$ falls within 0.9-1.0 range and is expected to adopt the perovskite structure in the solid state. This implies that the cations, MA^+ and Si^{2+} have identical size for the formation of a cubic perovskite structure. The tolerance factor of $MASiI_3$ is comparable to that of $MAPbI_3$ having a value of 0.91. The octahedral factor $\mu = r_{Si}/r_I$ calculated as 0.51 for $MASiI_3$ fall within the range 0.442-0.895 expected for stable perovskites (Li *et al*, 2008). This is also comparable to that of $MAPbI_3$ (0.54). The tolerance factor and octahedral factor combination (*t*, μ) define the perovskite region in the parameter space for perovskite structure formation.

Electronic properties of $MASiI_3$:

$MASiI_3$ behaves as a semiconductor with well-defined band gap between the conduction band and valence band. Band gap is an important electronic property of any perovskite since it directly links to its application as photovoltaics. In order to obtain an accurate band gap of $MASiI_3$, the band gap of $MAPbI_3$ was first calculated as 1.29 eV using GGA-PBEsol. Comparing with experimental value given as 1.51 eV, the GGA-PBEsol represent a gross underestimation in that electronic property. This makes PBEsol unsuitable for band structure calculation. With GGA-HTCH/407, the band gap for $MAPbI_3$ was obtained as 1.483 eV giving an error less than 2% (0.027 eV) in the band gap prediction when compared to experimental value. Therefore HTCH/407 has a much greater universality and because of this high accuracy, GGA-HTCH/407 was used to compute the band structure of $MASiI_3$ and is given as 1.008 eV. Figure 2 shows the band structure of $MASiI_3$ and $MAPbI_3$. A careful evaluation shows close resemblance in the band structure of $MASiI_3$ and $MAPbI_3$ indicating silicon as an effective replacement for Pb in HOIPs.

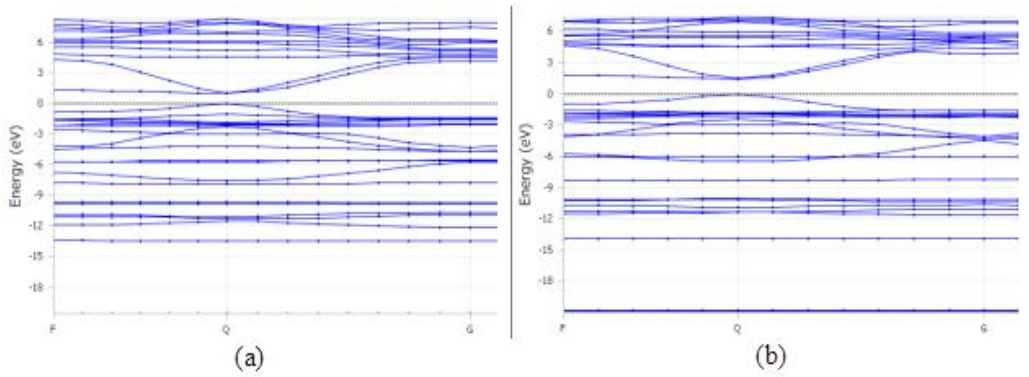

Figure 2: GGA-HTCH/407 calculated band structure along the F→Q→ G(Γ) → Z→ F (a): $MASiI_3$ (b): $MAPbI_3$

$MASiI_3$ is a direct band gap semiconductor similar to $MAPbI_3$. This means that the valence band maximum (VBM) and the conduction band minimum (CBM) occur virtually at the same point (Q-point) in the Brillouin zone. The VBM and CBM in cubic $MASiI_3$ and $MAPbI_3$ occur at a Brillouin zone boundary (the Q point). By mapping the band structure parameters on the energy scale (Fig. 3), the position of Fermi level which is a crucial factor in determining electrical properties, can be easily established. It is clear that the Fermi level in $MASiI_3$ is closer to the conduction band indicating an *n*-type extrinsic behavior. This behavior is characterized by loosely bound electrons in the valence band that can be easily excited into the conduction band. Hence, conduction is by the movement of electrons in the conduction band. Also, it will require very little energy for the electrons to go to the conduction band. In

comparison, $MAPbI_3$ has Fermi level almost midway between the conduction band and valence band. This indicate that $MAPbI_3$ is an intrinsic semiconductor.

In order to determine the various contributions to the band energies around the fundamental band gap, the DOS and PDOS were calculated (Fig. 4). The valence band consists mostly of I p states with some admixture of Si *s* and *p* states and the conduction band consists primarily of Si states. The dominance of conduction band by the Si states (cation) is much expected for an ionic material with a valence band dominated by anion electronic states. Contributions from MA (the organic molecule) appear several electronvolts below the valence band maximum signifying little electronic interaction between the organic part (MA) and the inorganic Si part.

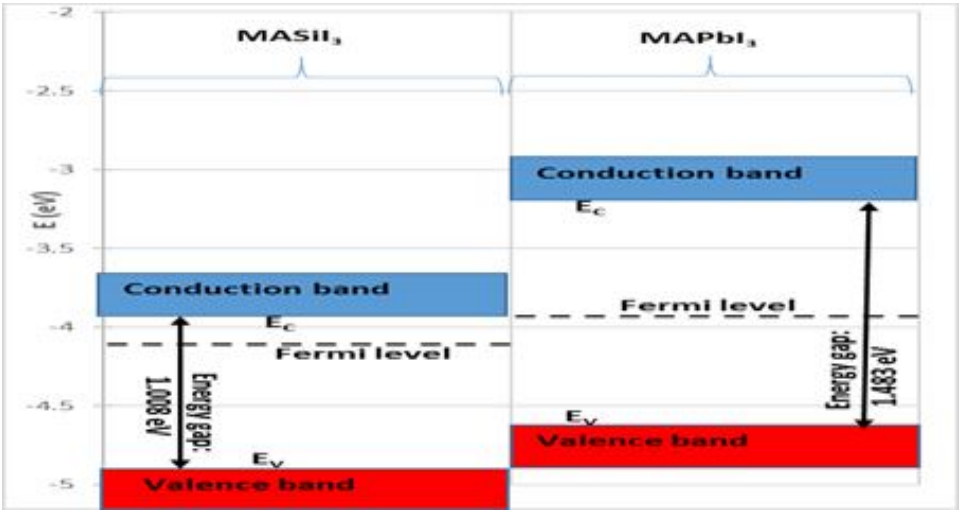

Figure 3: Band parameters of $MASiI_3$ compared to $MAPbI_3$. E_v is the valence band edge; E_c is the conduction band edge.

Optical properties of $MASiI_3$:

Figure 5 shows the optical absorption of $MASiI_3$. There are two intense absorptions in the visible and ultraviolet regions observed at 542 nm and 285 nm, respectively. This is important in order to trap energy spanning the entire region of UV/Visible spectrum. The striking result is the high value of absorption coefficient (α) in the range 6.40-7.14 x 10^4 for the observed absorptions between 285-542 nm and 1.75-1.88 x 10^5 nm in the region less than 200 nm. The high optical absorption coefficient enables high efficiency HOIPs-based thin film solar cells with rather thin absorbers, typically less than 500 nm. Comparing with $MAPbI_3$ (774 nm), the absorption of $MASiI_3$ is blue shifted. This can be tuned to higher wavelength through doping with other halide atoms such as Br and Cl which are known to cause a red shift and increase the band gap in HOIPs. The calculated optical absorption of $MAPbI_3$ agrees well with experimental value of ~ 800 nm and high absorption coefficient of about 10^5 nm for a thin film absorber layer.

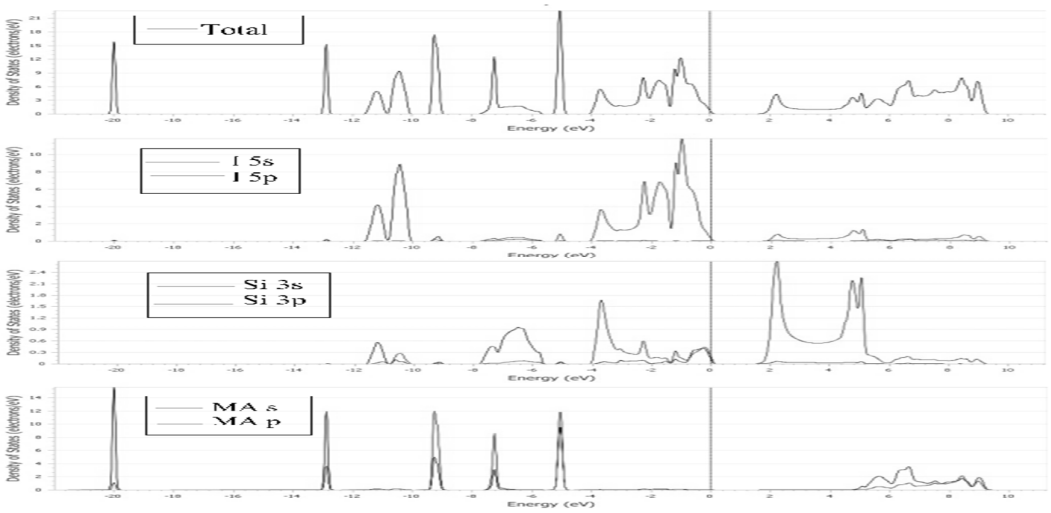

Figure 4: Calculated density of states (DOS) for cubic $MASiI_3$ showing contributions to each band

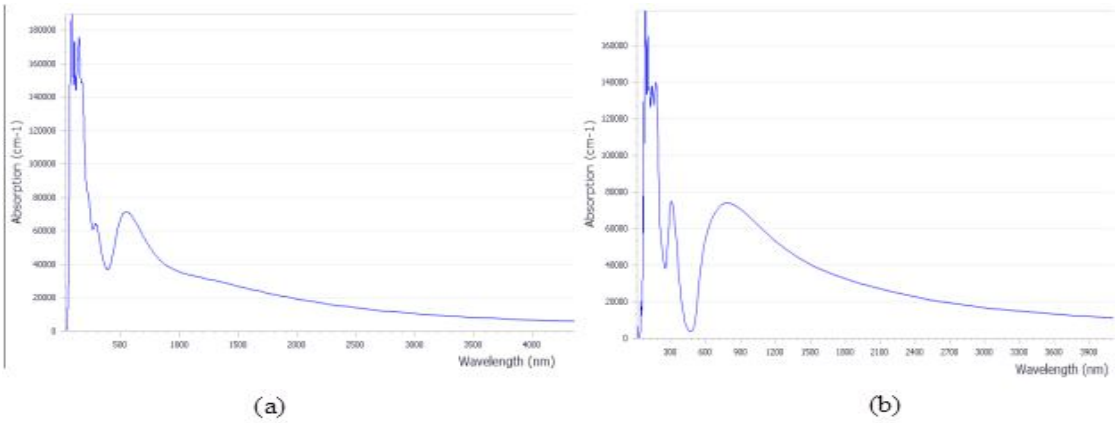

Figure 5: Theoretical Absorption spectrum (a): $MASiI_3$ (b): $MAPbI_3$

CONCLUSION AND RECOMMENDATION

$MASiI_3$ can effectively replace $MAPbI_3$ as solar energy absorber in solar cell technology. The Goldschmidt tolerance factor for Si^{2+} as B-site atom in silicon halide (iodide) perovskite is well accommodated within the range for the formation of stable perovskite structure. $MASiI_3$ is a direct band gap semiconductor with a band gap suitable for solar energy harvesting. The Fermi level indicates *n*–type extrinsic behavior. The high optical absorption within visible and ultraviolet regions shows that solar energy can be trapped across the whole sunlight energy spectrum

REFERENCES

Arkan, F. and Izadyar. M. (2018). Computational modeling of the photovoltaic activities in $EABX_3$ (EA=ethylammonium, B=Pb, Sn, Ge, X=Cl, Br, I) perovskite solar cells. *Computational Materials Science*, 152: 324–330.

Bhagwan. P. (2005). *A handbook of Inorganic Chemistry*, International Scientific Publishing Academy, New Delhi, India, P. 300.

Boese, A. D. and Handy, N. C. (2001). A new parametrization of exchange-correlation generalized gradient approximation functionals. The *Journal of Chemical Phys*ics, 114: 5497-5503.

Bryant, D., Aristidou, N., Pont, S., Sanchez-Molina, I., Chotchunangatchaval, T., Wheeler, S., Durrant, J. R. and Haque, S. A. (2016). Light and oxygen induced degradation limits the operational stability of methylammonium lead triiodide perovskite solar cells. *Energy and Environmental Science*, 9: 1655–1660.

Chan, S., Wu, M., Lee, K., Chen, W., Lin, T. and Su, W. (2017). Enhancing perovskite solar cell performance and stability by doping barium in methylammonium lead halide. *Journal of Materials Chemistry A*, 5: 18044-18052.

Clark, S. J., Segall, M. D., Pickard, C. J., Hasnip, P. J., Probert, M. J., Refson, K. and Payne, M. C. (2005). First principles methods using CASTEP. *Zeitschrift fur Kristallographie – Crystalline Materials*, 220: 567-570.

Delley, B. (2000). From molecules to solids with $Dmol^3$ approach. *Journal of Chemical Physics*, 113: 7756-7764.

Delley, B. (2006). Ground-state enthalpies: evaluation of electronic structure approaches with emphasis on the density functional method. The *Journal Physical Chemistry A*, 110: 13632-13639.

D'Innocenzo, V., Grancini, G., Alcocer, M. J. P., Kandada, A. R. S., Stranks, S. D., Lee, M. M., Lanzani, G., Snaith, H. J. and Petrozza, A. (2014). Excitons versus free charges in organo-lead tri-halide perovskites. *Nature Communications*, 5: 3586-3591.

Glazer, A. M. (1972). The classification of tilted octahedral in perovskites.*Acta Crystallographica Section B*, 28: 3384–3392.

Hodes, G. (2013). Perovskite-Based Solar Cells. *Science*, 342: 317–318.

Juarez-Perez, E. J., Hawash, Z., Raga, S. R., Ono, L. K. and Qi, Y. (2016). Thermal degradation of $CH_3NH_3PbI_3$ perovskite into NH_3 and CH_3I gases observed by coupled thermogravimetry–mass spectrometry analysis. *Energy and Environmental Science*, 9: 3406–3410.

Kieslich,G., Sun, S. and Cheetham,A. K. (2014). Solid-state principles applied to organic-inorganic perovskites: new trick for old dog.*Chemical Science*, 5: 4712–4715.

Kohn, W. and Sham, L. J. (1965). Self-consistent equations including exchange and correlation effects. *Physical Review*, 140: A1133-A1138.

Kojima, A., Teshima, K., Shirai, Y. and Miyasaka, T. (2009). Organometal halide perovskites as visible-light sensitizers for photovoltaic cells. *Journal of the American Chemical Society*, 131: 6050-6051.

Krishnamoorthy, T., Ding. H., Yan, C., Leong, W. L., Baikie, T., Zhang, Z., Sherburne, M., Li, S., Asta, M., Mathews, N. and Mhaisalkar, S. G. (2015). Lead-free germanium iodide perovskite materials for photovoltaic applications. *Journal of Materials Chemistry A*, 3: 23829-23832.

Lee, M. M., Teuscher, J., Miyasaka, T., Murakami, T. N. and Snaith, H. J. (2012). Efficient hybrid solar cells based on meso-superstructured organometal halide perovskites. *Science*, 338: 643-647.

Li, C., Lu, X., Ding, W., Feng, L., Gao, Y. and Guo, Z. (2008). Formability of ABX_3 (X = F, Cl, Br, I) halide perovskites. *Acta Cryst. Section B*, 64, 702–707.

Liu, X., Hong, R. and Tian, C. (2009). Tolerance factor and the stability discussion of ABO_3-type ilmenite. *Journal of Materials Science: Materials in Electronics*, 20 (4): 323–327.

Manser, J. S., Christians, J. A. and Kamat, P. V. (2016). Intriguing optoelectronic properties of metal halide perovskites.*Chemical Reviews*, 116: 12956-13008.

Matteocci, F., Cinà, L., Lamanna, E., Cacovich, S., Divitini, G., Midgley, P. A., Ducati, C. and Di Carlo, A. (2016). Encapsulation for long-term stability enhancement of perovskite solar cells. *Nano Energy*, 30: 162–172.

Monkhorst, H. J. and Pack, J. D. (1976). Special points for Brillouin-zone integrations. *Physical Review B*, 13:5188-5192.

Mosconi, E., Amat, A., Nazeeruddin, M. K., Grätzel, M. and Angelis, F. D. (2013). The *Journal of Physical Chemistry C*, 117: 13902–13913.

Navas, J., Sanchez-Coronilla, A., Gallardo, J. J., Martın, E. I., Hernandez, N. C., Alcantara, R., Fernandez-Lorenzoa, C. and Martın-Calleja, J. (2015). Revealing the role of Pb^{2+} in the stability of organic–inorganic hybrid perovskite $CH_3NH_3Pb_{1-x}Cd_xI_3$: an experimental and theoretical study. *Physical Chemistry Chemical Physics*, 17: 23886-23896.

Noel, N. K., Stranks, S. D., Abate, A., Wehrenfennig, C., Guarnera, S., Haghighirad, A., Sadhanala, A., Eperon, G. E., Pathak, S. K., Johnston, M. B., Petrozza, A., Herz, L. M. and Snaith, H. J. (2014). Lead-free organic–inorganic tin halide perovskites for photovoltaic applications. *Energy and Environmental Science*, 7: 3061-3068.

Perdew, J. P., Ruzsinszky, A., Csonka, G., Vydrov, O. A., Scuseria, G. E., Constantin, L. A., Zhou, X. and Burke, K. (2008). Restoring the density-gradient expansion for exchange in solids and surfaces.*Physical Review Letters*, 100: 136406(4).

Ponseca, C. S., Savenije, T. J., Abdellah, M., Zheng, K., Yartsev, A., Pascher, T., Harlang, T., Chabera, P., Pullerits, T., Stepanov, A., Wolf, J. P. and Sundström, V. (2014). Organometal halide perovskite solar cell materials rationalized: ultrafast charge generation, high and microsecond-long balanced mobilities, and slow recombination, *Journal of* the *American Chemical Society*, 136: 5189-5192.

Pulay, P. (1982). Improved SCF convergence acceleration, *Journal of Computational Chemistry*, 3: 556-560.

Sampson, M. D. Park, J. S. Schaller, R. D. Chan, M. K. Y. and Martinson, A. B. F. (2017). Transition metal-substituted lead halide perovskite absorbers. *Journal of Materials Chemistry A*, 5: 3578-3588.

Shai, X., Zuo, L., Sun, P., Liao, P., Huang, W., Yao, E., Li, H., Liu, S., Shen, Y., Yang, Y. and Wang, M. (2017). Efficient planar perovskite solar cells using halide Sr-substituted Pb perovskite. *Nano Energy*, 36: 213-222.

Shannon,R. D. (1976). Revised effective ionic radii and systematic studies of interatomic distances in halides and chalcogenides. *Acta Crystallographica Section A*, 32: 751–767.

Stoumpos,C. C., Malliakas,C. D. and Kanatzidis,M. G. (2013). Semiconducting tin and lead iodide perovskites with organic cations: phase transitions, high mobilities, and near-infrared photoluminescent properties. *Inorganic Chemistry*, 52: 9019-9038.

Stranks, S. D., Eperon,G. E., Grancini,G., Menelaou,C., Alcocer,M. J. P., Leijtens,T., Herz,L. M., Petrozza, V. and Snaith,H. J. (2013). Electron-hole diffusion lengths exceeding 1 micrometer in an organometal trihalide perovskite absorber. *Science*, 342: 341-344.

Yang, W.S., Noh, J. H., Jeon, N. J., Kim, Y. C., Ryu, S., Seo, J. and Seok, S. I. (2015). High-performance photovoltaic perovskite layers fabricated through intramolecular exchange. *Science*, 348: 1234-1237.

Yuan, Y., Wang, Q., Shao, Y., Lu, H., Li, T., Gruverman, A. and Huang, J. (2016). Electric-field-driven reversible conversion between methylammonium lead triiodide perovskites and lead iodide at elevated temperatures. *Advanced Energy Materials*, 6: 1501803 - 1501809.